Frequency measurement of the $^2S_{1/2}$-$^2F_{7/2}$ electric octupole transition in a single $^{171}Yb^+$ ion

K. Hosaka,[1,*] S. A. Webster,[1] A. Stannard,[1,2] B. R. Walton,[1] H. S. Margolis,[1] and P. Gill[1,2,3]
[1]*National Physical Laboratory, Hampton Road, Teddington, Middlesex TW11 0LW, United Kingdom*
[2]*Department of Physics, Clarendon Laboratory, University of Oxford, Oxford OX1 3PU, United Kingdom*
[3]*Blackett Laboratory, Imperial College London, South Kensington Campus, London SW7 2BZ, United Kingdom*
(Received 31 October 2008; published 10 March 2009)

We report on precision laser spectroscopy of the $^2S_{1/2}(F=0)$-$^2F_{7/2}(F=3,m_F=0)$ clock transition in a single ion of $^{171}Yb^+$. A linewidth of <40 Hz is observed and frequency instability due to fluctuation of the ac Stark shift is reduced through improved stability of the beam alignment. The absolute value of the transition frequency, determined using an optical frequency comb, is 642 121 496 772 657 ± 12 Hz with a fractional uncertainty of 2×10^{-14}. This is a factor of 50 better than the previously published value [Hosaka *et al.*, IEEE Trans. Instrum. Meas. **54**, 759 (2005)].

DOI: 10.1103/PhysRevA.79.033403 PACS number(s): 37.10.Ty, 06.30.Ft, 32.30.Jc

I. INTRODUCTION

The accuracy of laser spectroscopy has dramatically increased since the introduction of mode-locked octave-spanning femtosecond laser combs for relating optical frequencies directly to the caesium primary standard [1]. Development in the stabilization of lasers to high finesse Fabry-Perot cavities has also led to greatly improved resolution, and subhertz laser linewidths have been reported in several laboratories [2–4]. In combination with these techniques, many optical frequency standards based on narrow linewidth forbidden transitions in either laser-cooled single ions or neutral atoms are currently being developed worldwide, and systematic uncertainties of 10^{-16} and below [5,6] have now been achieved. Optical frequency standards have the potential to reach fractional uncertainties below 10^{-17}, and reproducibility proven at this level would open up the possibility of a primary standard for time based on an optical clock. A number of different candidate ion and atom species are being investigated at various national standards laboratories and research institutes. These include electric quadrupole transitions in mercury [7], strontium [8,9], ytterbium [10] and calcium ions [11], and hyperfine-induced electric-dipole $^1S_0$-$^3P_0$ transitions in indium [12] and aluminum [13] ions and in neutral strontium [5,14,15], ytterbium [16–18], and mercury [19,20] atoms.

The term scheme for the 171 isotope of singly-ionized ytterbium is shown in Fig. 1. The ytterbium ion has the unique feature that its lowest-lying excited state is an F state, having an orbital angular momentum, $l=3$. This can only decay to the ground state by electric octupole radiation and is therefore extremely long lived, having a lifetime of approximately 6 yr [21,22]. Consequently, the S-F transition at 467 nm has a natural linewidth on the order of nanohertz, which affords the advantage that spectroscopic resolution and the stability of the frequency standard will not be limited by the atomic transition but rather by the linewidth and stability of the probe laser. A further advantage of the octupole transition is its low sensitivity to external fields. It has zero linear Zeeman shift and a fractional second-order shift of -3×10^{-18} μT^{-2} [23], the smallest known quadrupole moment of any alkalilike ion, $Q=-0.2ea_0^2$ [24,25], and a fractional blackbody Stark shift of -2.5×10^{-16} [26] at 300 K, one of the smaller for the ion species under investigation and equal to the smallest known for neutral atoms [20]. Due to the relatively high intensity required to drive the octupole transition, there is an appreciable ac Stark shift from the probe laser [27] and this is currently the dominant systematic effect. However, on reduction in the probe-laser linewidth, the intensity may be reduced while maintaining the same probability of excitation and we project that the uncertainty in the ac Stark shift may be reduced to below the 10^{-17} level.

The accuracy of previous measurements of the transition was limited by the observed atomic absorption linewidth [28] and the instability of the dominant systematic effect, which is the ac Stark shift [23]. In Sec. II, we describe im-

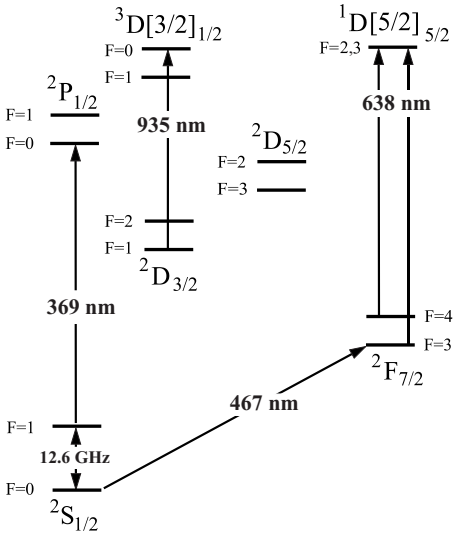

FIG. 1. Schematic energy-level diagram of $^{171}Yb^+$, showing the cooling transition at 369 nm and the $^2S_{1/2}$-$^2F_{7/2}$ optical clock transition at 467 nm. The metastable $^2D_{3/2}$ and $^2F_{7/2}$ states are depopulated by laser radiation at 935 and 638 nm, respectively. Microwaves at 12.6 GHz mix the hyperfine levels of the ground state.

*Present address: National Metrology Institute of Japan, Tsukuba Central 3, Umezono 1-1-1, Tsukuba 305-8563, Japan.

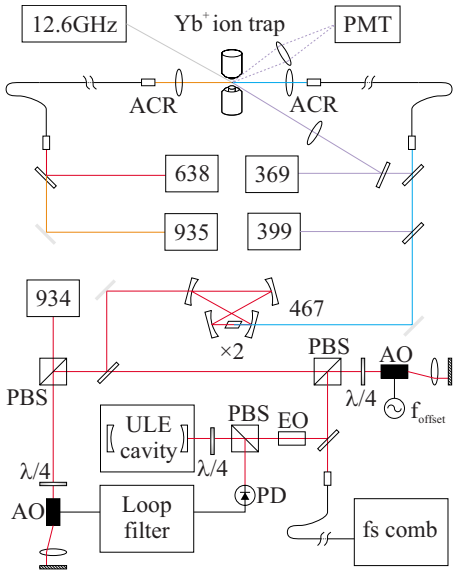

FIG. 2. (Color online) Experimental setup showing probe-laser system and beam delivery to the ion trap. The frequency of the light at 467 nm, $f_{467}=2(f_{\text{cavity}}+2f_{\text{offset}})$, where f_{cavity} is the cavity frequency and f_{offset} is the frequency offset to the cavity. ACR, achromatic lens; AO, acousto-optic modulator; EO, electro-optic modulator; λ/4, quarter-wave plate; PBS, polarizing beam splitter; PD, avalanche photodiode; PMT, photomultiplier tube. The laser systems are represented by boxes showing their wavelength in nanometers.

proved techniques for probe beam alignment that reduce the instability of the ac Stark shift and report a reduced atomic absorption linewidth of 40 Hz. In Sec. III, we report an improved measurement of the frequency of the electric octupole transition in a single $^{171}Yb^+$ ion using a femtosecond laser frequency comb. As a result of the experimental improvements, we have achieved a factor of 50 reduction in uncertainty compared to the previously published value for this transition frequency.

II. EXPERIMENT

A diagram of the experimental setup is shown in Fig. 2. A Paul trap of the endcap design [29] is used to trap a single ytterbium ion. A radio frequency voltage at 14 MHz, with an amplitude of 300 V, is applied to the endcaps resulting in harmonic-oscillator frequencies of 1–2 MHz. To load the trap, an atomic beam passes through the trapping region and ions are generated by photoionization with light at 399 nm [23]. The transitions used to laser cool and probe the ion are shown in Fig. 1. Doppler cooling is performed on the $^2S_{1/2}(F=1)$-$^2P_{1/2}(F=0)$ transition with light at 369 nm, generated by frequency doubling a Ti:sapphire laser. In the upper $^2P_{1/2}(F=0)$ level of the cooling transition, the ion can decay to the $^2D_{3/2}(F=1)$ level with a branching ratio of 7×10^{-3} [30] and so a 935 nm diode laser is used to return the ion to the $F=1$ ground state via the $^3D[3/2]_{1/2}(F=0)$ level. Although these transitions form a closed cooling cycle, it is possible for the ion to leave the cycle by a spontaneous Raman transition to the $F=0$ ground state via the $F=1$ level of the $^2P_{1/2}$ state. To maintain cooling, microwave radiation at 12.6 GHz is used to mix the $F=0$ and $F=1$ ground states. Prior to driving the octupole transition, the microwaves are switched off for 30 ms to prepare the ion in the $F=0$ ground state. Light at 467 nm is then used to drive the $^2S_{1/2}(F=0)$-$^2F_{7/2}(F=3,m_F=0)$ clock transition, and the fluorescence at 369 nm, detected by a photomultiplier tube in a 50 ms interval, is used to determine the ion state. Following excitation to the $^2F_{7/2}(F=3)$ level, a 638 nm diode laser excites the ion to the $^1D[5/2]_{5/2}$ state from which it decays back down to the ground state via the $^2D_{3/2}$ and $^2D_{5/2}$ states. Decay can also occur to the $F=4$ level of the $^2F_{7/2}$ state and so a second laser at 638 nm is used to depopulate this level.

The light at 467 nm is generated by frequency doubling a Ti:sapphire laser. The fundamental light at 934 nm is stabilized to an ultra-low-expansivity (ULE) cavity using the Pound-Drever-Hall technique [31]. An error signal is fed back to an external double-passed acousto-optic modulator (AOM) and with this a servo bandwidth of 250 kHz is achieved, which is sufficient to suppress the residual noise from the laser to a level where it no longer dominates the frequency noise of the stabilized light. Rather, this is determined by the frequency stability of the cavity. The ULE cavity has a free spectral range of 1.5 GHz and a finesse of 190 000. The cavity is housed within a vacuum chamber which is supported on a passive vibration isolation platform within an acoustic isolation box. With a two-layer temperature control, the magnitude of the frequency drift during daytime is typically <0.5 Hz/s, above a long-term isothermal drift of about 50 mHz/s. The frequency offset between the fundamental light and the nearest cavity fringe is bridged by a double-passed AOM; the drive frequency of which is provided by a computer-controlled frequency synthesizer. The probe laser is scanned in frequency by stepping this offset from the cavity. To determine its linewidth, light at 934 nm is independently stabilized to a second nominally identical cavity and the heterodyne beat between the light stabilized to the two cavities is measured. Figure 3 shows the resulting spectrum. The linewidth observed for a single 1 s acquisition period is 5 Hz [full width at half maximum (FWHM)] which then broadens to 20 Hz over 100 s. The sidebands at 100 and 150 Hz are harmonics of the frequency of U.K.'s electricity supply.

The transition at 467 nm is extremely weak and so the probe beam at this wavelength cannot be aligned by direct observation of the transition. Instead, a tracer beam at 369 nm is aligned on the ion by observation of fluorescence, and alignment of the probe beam is then ensured by overlapping it with the tracer. The accuracy and stability of these alignments are crucial to the operation of the experiment, affecting both the 467 nm transition rate and the ac Stark shift which both depend on the intensity at the ion. The overlap of the probe and tracer beams is guaranteed by coupling them into the same dual wavelength fiber and then bringing them to a focus at the same point with an achromatic lens. The fiber output and lens are mounted on a three-axis translation stage which is then adjusted to align the tracer on the ion. The spot size ($1/e^2$ radius) at the focus is 5 μm for the light at 467 nm (4 μm for the light at 369 nm) and the intensity at the ion can be varied by translating the lens and fiber along

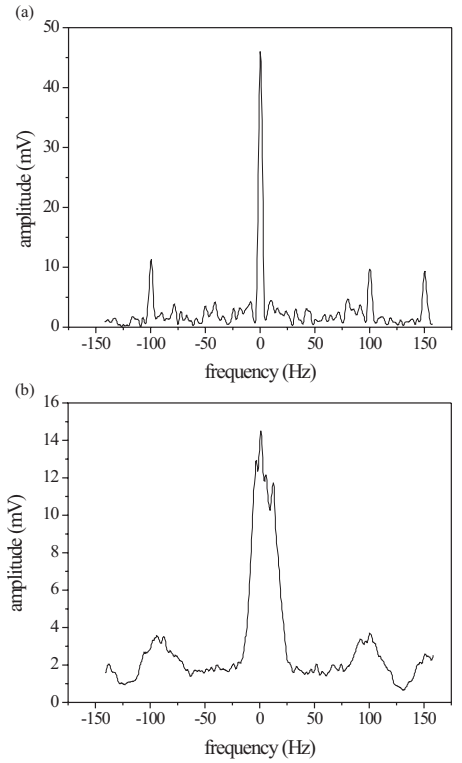

FIG. 3. Spectrum of the heterodyne beat between light locked to two independent cavities at 934 nm (a) after a 1 s acquisition and (b) on averaging for 100 s. The data were taken with a measurement bandwidth of 0.5 Hz.

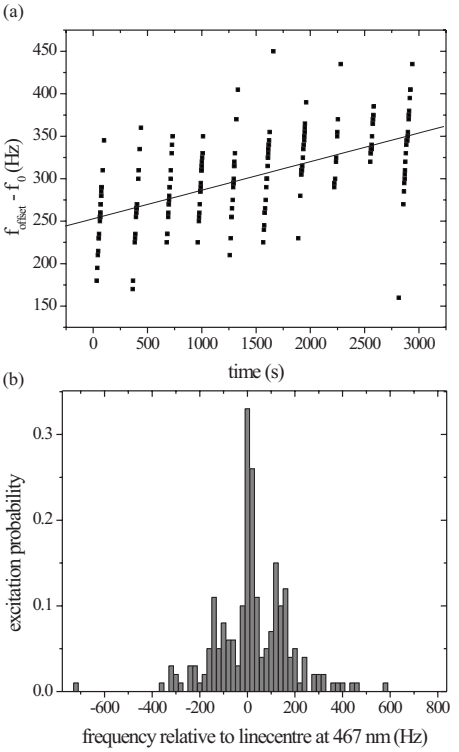

FIG. 4. (a) Plot showing the offset frequency corresponding to individual quantum jumps as a function of time for ten scans of the probe-laser frequency across the 467 nm transition. f_0 = 122 243 000 Hz in this figure. A linear fit to the data yields a slope of 33.7 mHz/s, corresponding to a cavity drift rate of 67.4 mHz/s. (b) The drift is removed and the data collated to give the atomic absorption spectrum of the clock transition at 467 nm. The measurement bandwidth is 20 Hz.

the optical axis, thus defocusing the beam. The power of the probe beam is stabilized by monitoring the output from the fiber and feeding back to an AOM on the fiber input, resulting in fluctuations below 0.1%. In the previous arrangement [27], the two wavelengths were made to overlap by ensuring their collinearity over a 5 m beam path in free space and by checking their transmission through a 5 μm pinhole. The overlapped beams were then aligned onto the ion using a beam steering mirror with differential micrometers. There was no power stabilization. Drift in both the overlap of the two beams and the alignment on the ion and fluctuations in power led to instability of the ac Stark shift and this can be seen in the scatter of the data in, for example, Fig. 2 of Ref. [23]. The stability and reproducibility of the current arrangement are much improved as evidenced by a significant reduction in the scatter of the data (see Sec. III). The transition at 638 nm, which is used to de-excite the ion from the F state, is also relatively weak, and the same alignment technique is employed using the beam at 935 nm as a tracer.

The probe laser is repeatedly scanned over the transition and the time and offset frequency at which quantum jumps occur are recorded. Figure 4(a) shows a data set made up of ten separate scans each consisting of 40 steps in the offset frequency of 5 Hz, and at each step there are ten interrogations of 50 ms. A linear least-squares fit to the data gives a slope of 33.7 mHz/s in the frequency offset which, as the offset is bridged by a double-passed AOM, corresponds to a cavity drift rate of 67.4 mHz/s. The drift is removed and the data are collated to give the profile shown in Fig. 4(b). Recalling that $f_{467}=2(f_{\text{cavity}}+2f_{\text{offset}})$, the offset frequency is multiplied by 4 to give the correct scale on the x axis in terms of the frequency at 467 nm. It should also be noted that the other Zeeman components and secular sidebands are well outside the range shown. A narrow carrier is observed, having a width of $<$40 Hz, which is comparable to the linewidth of the probe laser observed on a similar timescale, as shown in Fig. 3(b), taking into account the factor of 2 difference in the frequency scales at 934 and 467 nm. In previous measurements, the linewidth of the atomic absorption spectrum was 200 Hz [23], 1 order of magnitude greater than one would expect if broadening was due to the probe laser alone. A measurement of the motion of the trap was made by reflecting light directly off the electrodes and detecting the heterodyne beat with a frequency-shifted reference beam. The beat spectrum was found to have a linewidth of 200 Hz; thus, Doppler broadening due to the motion of the trap relative to the probe beam could account for the observed width [28]. The trap is constructed on an electrical feed through and this is bolted to a vacuum chamber which hangs from a steel platform, situated on an optical table. To improve the mechanical rigidity of the trap, the vacuum chamber is now supported from below by a mount fixed to the optical table, and the top of the pin of the electrical feed through, on which the trap is mounted, is clamped within the vacuum chamber. The Doppler broadening is now measured to be at a negli-

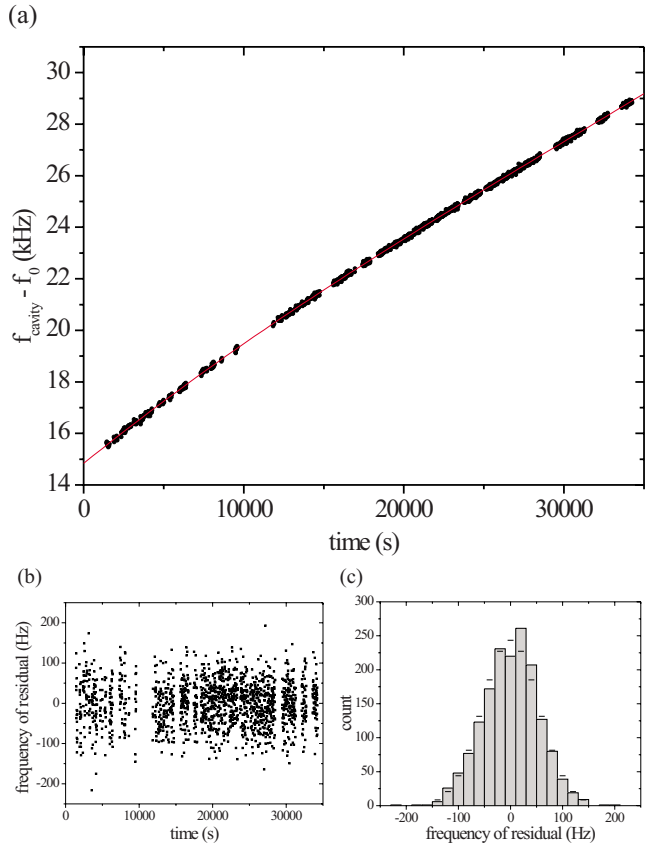

FIG. 5. (Color online) (a) Frequency of the ULE cavity fringe measured by the optical frequency comb using a counter gate time of 10 s. f_0=321 060 503 100 kHz in this figure. The solid line is a third-order polynomial fit to the data. The linear component of the cavity drift is 0.50 Hz/s. (b) Residuals of the fit. The standard deviation and standard error of the mean are 53 and 1.3 Hz, respectively. (c) Histogram of the residuals. The horizontal lines indicate the values expected for a normal distribution centered on 0 Hz with a width of 53 Hz.

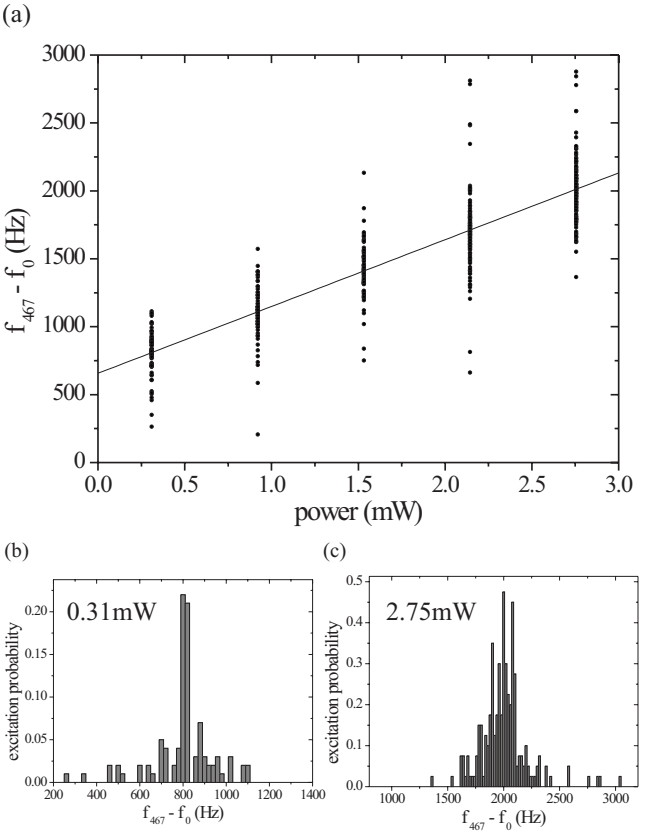

FIG. 6. (a) Frequency of the octupole transition as a function of probe-laser power. f_0=642 121 496 772 000 Hz in this figure. Each data point corresponds to an individual quantum jump. The solid line is a linear fit to all data points and has a slope of 492 Hz/mW. The data at (b) 0.31 and (c) 2.75 mW are collated and are shown as histograms.

gible level, $\ll 1$ Hz on the carrier, and the linewidth of the atomic absorption spectrum is limited by that of the probe laser.

III. ABSOLUTE FREQUENCY MEASUREMENT AND SYSTEMATIC SHIFTS

To perform a measurement of the absolute frequency, the probe laser is scanned over the octupole transition while the frequency of the light stabilized to the ULE cavity is measured simultaneously by the femtosecond laser frequency comb. The data-acquisition systems for the ion trap and the optical frequency comb both record the time and frequency during the measurement, and the data are subsequently combined. The clocks on the two systems are synchronized to within a second, and the synthesizer providing the cavity offset frequency and those used in the optical frequency comb are all referenced to the 10 MHz output of a hydrogen maser which forms part of the clock ensemble used to generate the NPL [coordinated universal time (UTC)] time scale. Figure 5(a) shows a sample set of data for the measurement of the frequency of the ULE cavity fringe by the optical frequency comb over a period of more than 9 h, and the solid line is a third-order polynomial fit to the data. Figure 5(b) shows the residuals of the fit and these have a standard deviation of 53 Hz. A histogram of the residuals is shown in Fig. 5(c) along with the values expected for a normal distribution centered on 0 Hz with a width of 53 Hz. The χ^2 value of the observed values is 15.0, and for 12 degrees of freedom, the probability that the χ^2 value exceeds this value is 24%. From this it is reasonable to conclude that the residuals are normally distributed and that the third-order polynomial is a good choice of model. On combining the ion trap and frequency comb data, the fit to the comb data is used to determine the absolute frequency of the cavity at the time of each quantum jump.

In addition to scanning the probe-laser frequency, the 467 nm power is also varied to calibrate the dominant systematic effect, the ac Stark shift. Data are taken at five different powers as shown in Fig. 6(a). The data points correspond to individual quantum jumps; the absolute frequencies of which are determined by the cavity frequency and the AOM offset frequency. At each power, the probe laser is repeatedly scanned in frequency over the transition until a hundred or more quantum jumps are accumulated. Each scan consists of 100 steps of 20 Hz in the transition frequency with ten inter-

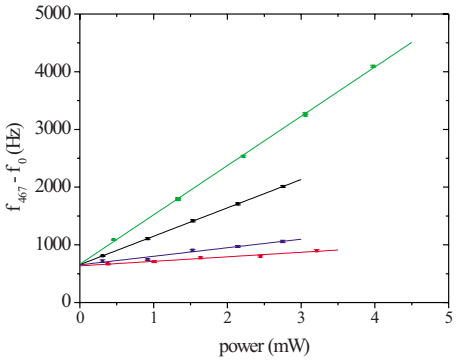

FIG. 7. (Color online) Frequency of the octupole transition as a function of probe-laser power for four different focusing conditions. f_0=642 121 496 772 000 Hz in this figure. Each data point is the mean of the quantum jump frequencies at a particular power and spot size [for example the data shown in Figs. 6(b) and 6(c)], and the standard error is shown. The solid lines are linear fits to the data for each focusing condition.

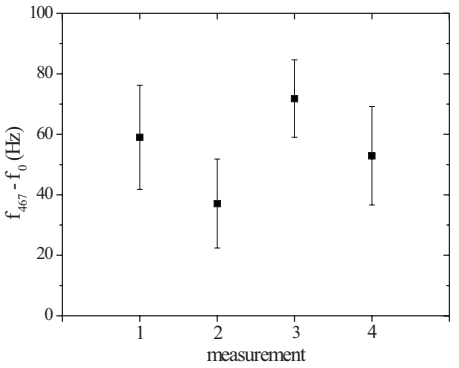

FIG. 8. Comparison of frequencies unperturbed by the ac Stark shift and corrected for maser offsets. f_0=642 121 496 772 600 Hz in this figure. Each data point is the zero-power intercept of a fit to individual quantum jumps as shown for example in Fig. 6(a). The error bars are those corresponding to the error on the intercept of the fit. Corrections for the deviation of the maser frequency from 10 MHz, as determined by comparison with UTC, are included.

rogations of 50 ms at each step. A linear fit to all data points yields a slope of 492 Hz/mW with an intercept of 657 ± 17 Hz. Histograms of quantum jump profiles at 0.31 and 2.75 mW are shown in Figs. 6(b) and 6(c), respectively. The linewidth of the carrier at 2.75 mW is greater than that at 0.31 mW due to power broadening.

It would be preferable to stabilize the frequency of the probe laser to the atomic transition and to measure this frequency with the femtosecond comb. However, given the structure in the atomic spectrum, there is a possibility that the laser will lock onto a sideband. A pulse of 5 ms, with a Fourier-transform-limited width of 200 Hz, would wash out the sidebands but would result in a much larger ac Stark shift, given the higher intensity required to excite the transition with the same probability. Therefore, the less efficient but more reliable method of continually scanning over the transition and building up a histogram of quantum jumps is used for making the measurement.

As a further check on the ac Stark shift calibration, the measurement is repeated for four different focusing conditions as shown in Fig. 7. The means of the quantum jump data at each power are shown with standard errors, and the straight lines are linear fits to each data set. The scatter of the data is significantly reduced compared to previous measurements due to the improved stability and reproducibility of the probe beam alignment.

To obtain the frequency unperturbed by the ac Stark shift, the data are extrapolated to zero power. Figure 8 shows the zero-power intercepts for the four measurements. Each point is the intercept of the unweighted fit to the individual quantum jump data, as shown for example in Fig. 6(a). The values also include corrections for the deviation of the maser reference frequency from 10 MHz as determined by comparison with UTC. The four data sets were taken over a number of days, and a different maser correction, of between 1 and 2 Hz, is applied to each point with an uncertainty of 1×10^{-14} or 6.4 Hz. A weighted mean of the four points gives, for the frequency of the transition that is unperturbed by the ac Stark shift and corrected for maser offsets, a value of 642 121 496 772 656 $\pm$ 12 Hz. Given that the mean is derived from four values, a conservative estimate is made for the uncertainty by assuming the points to be rectangularly distributed and taking one standard error as being equal to the standard deviation. The other systematic effect that needs to be taken into account at this level of precision is the second-order Zeeman shift. A field of 24 ± 8 μT is applied during the probe pulse, and when combined with a coefficient of -1.72 ± 0.03 mHz μT^{-2} [23], this gives a second-order Zeeman shift of $-1.0^{+0.8}_{-0.6}$ Hz. Correcting for this shift gives a value of 642 121 496 772 657 $\pm$ 12 Hz for the frequency of the $^2S_{1/2}(F=0)$-$^2F_{7/2}(F=3, m_F=0)$ transition in $^{171}Yb^+$.

Other systematic effects include the quadrupole shift, the blackbody shift, the second-order Doppler shift and the dc Stark shift but do not contribute significantly at this level. However, for completeness, they are included in Table I which summarizes the size and standard uncertainty of all the shifts. The uncertainty estimate for the quadrupole shift is based on there being a stray mean dc potential on the inner endcap electrodes relative to the outer endcap electrodes of

TABLE I. Systematic shifts and their standard uncertainties. Corrections for ac Stark effect and maser offset are applied to the data points shown in Fig. 8 and these shifts are therefore not included in this table.

Shift	$\Delta\nu$ (Hz)	σ_ν (Hz)
Statistical and ac Stark		9.8
Maser frequency		6.4
Second-order Zeeman	−1.0	0.8
Quadrupole	0.2	0.4
Blackbody Stark	−0.15	0.07
Doppler	0.0	0.05
dc Stark	−0.04	0.04
Total	−1.0	11.7

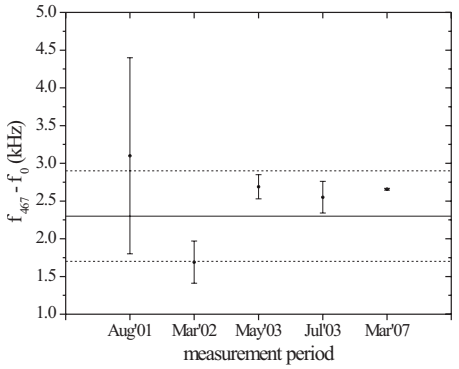

FIG. 9. Comparison of measurements of the $^2S_{1/2}(F=0)$-$^2F_{7/2}(F=3, m_F=0)$ transition frequency over a period of several years. $f_0=642\ 121\ 496\ 770$ kHz in this figure. Each data point is the mean at the time of measurement and the standard error (1σ) is shown. The solid line is the value for the mean of the measurements made in the period 2001–2003, and the dashed lines are the mean plus and minus one standard errors.

± 1 V, giving rise to an electric quadrupole field gradient of $\pm 4 \times 10^{-6}$ V m^{-2}. This couples to the quadrupole moment of the $^2F_{7/2}$ state, which is calculated to be $-0.2ea_0^2$ [25], and taking into account that the B field is at 90° to the trap axis, this gives an uncertainty of ± 0.4 Hz. The nonzero shift is due to the application of a small known dc voltage to one of the outer endcap electrodes to minimize the micromotion of the trapped ion.

The absolute frequency of the electric octupole transition has previously been measured four times with a femtosecond laser frequency comb [32] and these values are plotted together with the result of this work in Fig. 9. The global mean of the four measurements made in the period 2001–2003 is shown as a solid line, and the mean plus and minus one standard errors are shown as dashed lines. The result of this work is in good agreement with the global mean and the measurements made in 2001 and 2003. There is a 3.5σ discrepancy with the value obtained in 2002 and this may be due to an underestimation of the uncertainty of the ac Stark shift correction at that time. The present value of the frequency is now a factor of 50 better than the previous published value [23] and has a fractional uncertainty of 2×10^{-14}.

IV. SUMMARY AND OUTLOOK

This paper has reported on the precision spectroscopy of the electric octupole transition in a single trapped $^{171}Yb^+$ ion. Through improved rigidity of the trap structure and the subsequent reduction in trap vibrations relative to the laser, octupole transition linewidths of <40 Hz have been observed. The introduction of a different alignment scheme for the probe beam, employing a dual wavelength optical fiber and an achromatic lens for 467 and 369 nm, and stabilization of the output power from the fiber have led to much improved stability and reproducibility of the probe-laser intensity at the ion. Consequently, there is less fluctuation of the ac Stark shift leading to reduced scatter and statistical uncertainty in the data. Due to these technical improvements, the precision of the measurement has significantly increased, and we report a value for the frequency with an uncertainty of 12 Hz, a 50-fold improvement on the previous published value.

Further improvement and evaluation of the probe-laser linewidth are required to obtain improved stability and accuracy of the frequency standard. In particular, the stability of the passive optical cavity that controls the laser frequency must be improved. To this end, two optical cavities are being modified according to the vibration insensitive design previously developed and demonstrated at NPL [33]. Measurement of the coefficient of thermal expansion (CTE) is also underway, and the temperature of zero expansion for one cavity has been determined to be 3 °C. By reducing the effects of vibrations and controlling the temperature at the zero of the CTE, it is expected that the laser stability will be limited by the thermal noise of the cavity mirrors, to the 10^{-15} level for averaging times in the range of 0.5–100 s [34]. With this level of stability, reaching an atomic transition frequency stability of a part in 10^{-17} will require that the atomic signal is averaged for a period of around 1 day.

In addition to determining the stability of the standard, laser linewidth also affects the size of the dominant systematic effect, the ac Stark shift. The ac Stark shift is proportional to the intensity, I, while the excitation rate is proportional to the spectral intensity, which is itself proportional to I/Γ, where Γ is the spectroscopic linewidth. The excitation probability for a pulse of duration t is proportional to It/Γ. Usually, one operates in the Fourier-transform-limited regime, where the pulse duration is such that the transform-limited linewidth, $\Gamma_{\mathrm{FT}} \propto 1/t$, is broader than the laser linewidth, and in this case, the excitation probability is proportional to I/Γ_{FT}^2. Typically, the resonant excitation probability is optimized, and with this fixed, one can infer a scaling law for the ac Stark shift with linewidth $\Delta\nu_{\mathrm{ac\ Stark}} \propto \Gamma_{\mathrm{FT}}^2$.

The extent to which the transform-limited linewidth may be reduced is limited by the frequency flicker floor of the laser due to thermal noise. This sets an upper limit on the maximum pulse duration that may be used in acquiring sufficient data to stabilize the laser frequency to the atomic transition without degrading stability [35]. For a Fourier-transform-limited linewidth of 40 Hz (pulse duration of ≈ 25 ms), an intensity of 2 kW cm^{-2} is required to excite the transition with 50% probability, and at this intensity, the ac Stark shift is 600 Hz. For a laser with a stability of 1×10^{-15} for averaging times in the range of 0.5–100 s, a reasonable upper limit for the pulse length, allowing ~ 10 s to accumulate data, would be 250 ms, which has a Fourier limited linewidth of ≈ 4 Hz. Using the above scaling law for the ac Stark shift, this gives a fractional shift of 1×10^{-14}. The uncertainty in the ac Stark shift is dominated by the stability and accuracy of the alignment. Currently, this is $\sim 1\%$ of the size of the shift applied for calibration. On extending the pulse length, the intensity may be reduced by defocusing the beam, with the effect of reducing sensitivity to alignment. Calibration of the shift at the 0.1% level is feasible, which would then give an uncertainty of 1×10^{-17}. Clearly, it would be desirable to extend the pulse duration further, and for this, it will be necessary to lower the flicker

floor of the laser. This may be achieved by extending the cavity length and using silica as the mirror substrate material [36].

The quadrupole shift may be nulled by setting the dc electric quadrupole field to zero, which can be achieved by monitoring the secular frequencies of the ion in the trap [37]. In addition, one can null any residual shift by averaging the transition frequency over three orthogonal magnetic-field directions, in which case the shift sums to zero [38]. An intriguing alternative presents itself for the $^2F_{7/2}(F=3)$ level; the shift is proportional to the identity

$$\begin{pmatrix} F & 2 & F \\ -M_F & 0 & M_F \end{pmatrix},$$

which, for $F=3$ and $M_F=\pm 2$, is equal to zero. Therefore, if one was to measure the mean of the $m_F=0-m_F=\pm 2$ components of the $^2S_{1/2}(F=0)$-$^2F_{7/2}(F=3)$ transition, this would be free from the quadrupole shift. These components do have a linear magnetic-field dependence, and a standard based on their mean may be limited by the stability of the magnetic field. However, they could still provide a useful means of calibrating the quadrupole shift on the magnetic-field-insensitive $m_F=0-m_F=0$ component.

The blackbody Stark shift at room temperature relative to 0 K is $(-2.5\pm 1.0)\times 10^{-16}$. This is calculated using theoretical oscillator strengths for transitions from the upper and lower atomic states. The uncertainty is dominated by the uncertainty in the difference between the scalar polarizabilities of the upper and lower atomic states and is estimated, indirectly, from an experimental measurement of the dc Stark shift of the 435 nm electric quadrupole transition in $^{171}Yb^+$ [10,26]. Further refinement of this measurement and a similar measurement for the electric octupole transition would improve our knowledge of the polarizabilities and reduce the uncertainty in the shift. The temperature dependence is -3×10^{-18} K^{-1}; thus, achieving uncertainty at the 10^{-17} level will also require accurate evaluation of the temperature and isotropy of the blackbody radiation field experienced by the ion.

ACKNOWLEDGMENT

This work was supported by the UK National Measurement System Pathfinder Metrology Program.

[1] S. A. Diddams, D. J. Jones, J. Ye, S. T. Cundiff, J. L. Hall, J. K. Ranka, R. S. Windeler, R. Holzwarth, T. Udem, and T. W. Hänsch, Phys. Rev. Lett. **84**, 5102 (2000).
[2] B. C. Young, F. C. Cruz, W. M. Itano, and J. C. Bergquist, Phys. Rev. Lett. **82**, 3799 (1999).
[3] S. A. Webster, M. Oxborrow, and P. Gill, Opt. Lett. **29**, 1497 (2004).
[4] A. D. Ludlow, X. Huang, M. Notcutt, T. Zanon-Willette, S. M. Foreman, M. M. Boyd, S. Blatt, and J. Ye, Opt. Lett. **32**, 641 (2007).
[5] A. D. Ludlow *et al.*, Science **319**, 1805 (2008).
[6] T. Rosenband *et al.*, Science **319**, 1808 (2008).
[7] W. H. Oskay *et al.*, Phys. Rev. Lett. **97**, 020801 (2006).
[8] H. S. Margolis, G. P. Barwood, G. Huang, H. A. Klein, S. N. Lea, K. Szymaniec, and P. Gill, Science **306**, 1355 (2004).
[9] P. Dubé, A. A. Madej, J. E. Bernard, L. Marmet, J. S. Boulanger, and S. Cundy, Phys. Rev. Lett. **95**, 033001 (2005).
[10] T. Schneider, E. Peik, and C. Tamm, Phys. Rev. Lett. **94**, 230801 (2005).
[11] M. Chwalla, J. Benhelm, K. Kim, G. Kirchmair, T. Monz, M. Riebe, P. Schindler, A. Villar, W. Haensel, C. Roos, R. Blatt, M. Abgrall, G. Santarelli, G. Rovera, and P. Laurent, Phys. Rev. Lett. **102**, 023002 (2009).
[12] Y. H. Wang, R. Dumke, T. Liu, A. Stejskal, Y. N. Zhao, J. Zhang, Z. H. Lu, L. J. Wang, T. Becker, and H. Walther, Opt. Commun. **273**, 526 (2007).
[13] T. Rosenband *et al.*, Phys. Rev. Lett. **98**, 220801 (2007).
[14] M. Takamoto, F.-L. Hong, R. Higashi, Y. Fujii, M. Imae, and H. Katori, J. Phys. Soc. Jpn. **75**, 104302 (2006).
[15] X. Baillard *et al.*, Eur. Phys. J. D **48**, 11 (2008).
[16] N. Poli *et al.*, Phys. Rev. A **77**, 050501(R) (2008).
[17] C. Y. Park and T. H. Yoon, Phys. Rev. A **68**, 055401 (2003).
[18] M. Yasuda, F.-L. Hong, T. Kohno, H. Inaba, K. Hosaka, C. Willis, T. Kurosu, A. Onae, and S. Ohshima, in Proceedings of the SPIE, Time and Frequency Metrology, 2007, edited by R. J. Jones, Vol. 6673, p. 66730D.
[19] H. Hachisu, K. Miyagishi, S. G. Porsev, A. Derevianko, V. D. Ovsiannikov, V. G. Pal'chikov, M. Takamoto, and H. Katori, Phys. Rev. Lett. **100**, 053001 (2008).
[20] M. Petersen, R. Chicireanu, S. T. Dawkins, D. V. Magalhães, C. Mandache, Y. Le Coq, A. Clairon, and S. Bize, Phys. Rev. Lett. **101**, 183004 (2008).
[21] M. Roberts, P. Taylor, G. P. Barwood, P. Gill, H. A. Klein, and W. R. C. Rowley, Phys. Rev. Lett. **78**, 1876 (1997).
[22] M. Roberts, P. Taylor, G. P. Barwood, W. R. C. Rowley, and P. Gill, Phys. Rev. A **62**, 020501(R) (2000).
[23] K. Hosaka, S. A. Webster, P. J. Blythe, A. Stannard, D. Beaton, H. S. Margolis, S. N. Lea, and P. Gill, IEEE Trans. Instrum. Meas. **54**, 759 (2005).
[24] P. J. Blythe, S. A. Webster, K. Hosaka, and P. Gill, J. Phys. B **36**, 981 (2003).
[25] P. Blythe, Ph.D. thesis, University of London, 2004.
[26] S. N. Lea, S. A. Webster, and G. P. Barwood, Proceedings of the 20th European Frequency and Time Forum, 2006 (PTB, Braunschweig, Germany), pp. 302-307.
[27] S. A. Webster, P. Taylor, M. Roberts, G. P. Barwood, and P. Gill, Phys. Rev. A **65**, 052501 (2002).
[28] S. A. Webster, A. Stannard, K. Hosaka, and P. Gill, in Proceedings of the 20th European Frequency and Time Forum, 2006 (PTB, Braunschweig, Germany), pp. 298-301.
[29] C. A. Schrama, E. Peik, W. W. Smith, and H. Walther, Opt. Commun. **101**, 32 (1993).
[30] B. C. Fawcett and M. Wilson, At. Data Nucl. Data Tables **47**, 241 (1991).
[31] R. W. P. Drever, J. L. Hall, F. V. Kowalski, J. Hough, G. M. Ford, A. J. Munley, and H. Ward, Appl. Phys. B: Photophys.

Laser Chem. **31**, 97 (1983).
[32] S. A. Webster, K. Hosaka, P. J. Blythe, H. S. Margolis, S. N. Lea, G. Huang, W. R. C. Rowley, and P. Gill, NPL Report No. CBTLM 28, 2003.
[33] S. A. Webster, M. Oxborrow, and P. Gill, Phys. Rev. A **75**, 011801(R) (2007).
[34] S. A. Webster, M. Oxborrow, S. Pugla, J. Millo, and P. Gill, Phys. Rev. A **77**, 033847 (2008).
[35] E. Riis and A. G. Sinclair, J. Phys. B **37**, 4719 (2004).
[36] K. Numata, A. Kemery, and J. Camp, Phys. Rev. Lett. **93**, 250602 (2004).
[37] G. P. Barwood, H. S. Margolis, G. Huang, P. Gill, and H. A. Klein, Phys. Rev. Lett. **93**, 133001 (2004).
[38] W. M. Itano, J. Res. Natl. Inst. Stand. Technol. **105**, 829 (2001).